Climate Dynamics
https://doi.org/10.1007/s00382-024-07328-6

ORIGINAL ARTICLE

Elevation dependent change in ERA5 precipitation and its extremes

Olivia Ferguglia[1] · **Elisa Palazzi**[1] · **Enrico Arnone**[1]

Received: 7 February 2024 / Accepted: 29 June 2024

Abstract
Mountain regions are recognised as hot-spots of climate change. Although the existence of an Elevation-Dependent Warming has been extensively confirmed in several mountain areas of the globe, fewer studies have analysed the elevational stratification of temporal trends of other climate variables, and particularly for precipitation. This study analyses changes in mean precipitation and its extremes in ERA5 global reanalysis data in key mountain areas of the globe, along with their elevational dependence, from 1951 to 2020. These include the Tibetan Plateau, the US Rocky Mountains, the Greater Alpine Region, and the Andes, as representative of different latitudes and climatic influences. Our analysis reveals common patterns of elevational dependent change in precipitation and its extremes in most of the mountainous areas, which emerge beyond their geographical differences. A positive elevational gradient of trends of extreme precipitation indices is found in the Tibetan Plateau, the Greater Alpine Region, and the subtropical Andes, highlighting a wetting effect (positive trends) at very high elevations. In contrast, the Rocky Mountains exhibit a negative elevational gradient, with a drying effect (negative trends) increasing with the elevation. Notably, a simple linear regression proved to be effective to describe the stratification of change in the Greater Alpine Region and the Rocky Mountains, whereas more complex vertical patterns need to be considered for the Andes and the Tibetan Plateau. Mean precipitation, heavy (≥10 mm) precipitation and the length of consecutive wet days show a consistent elevation-dependent stratification within each of the study areas, suggesting possible common driving mechanisms.

Keywords Precipitation extremes · Elevation dependent precipitation change · ERA5 reanalysis · Mountains · ETCCDI indices

1 Introduction

High elevation areas are attracting increasing attention of the scientific community as climate change hot-spots, or even sentinels, whose climatic equilibrium may be more rapidly altered compared to the majority of other regions, or to globally-averaged signals. Regarded as the "water towers" of the Earth (Viviroli et al. 2011), mountains are also crucial to the planet's hydrological cycle as they contribute to the seasonal and long-term storage of water resources for roughly half of the global population (Beniston 2003).

Over the last ten years, several studies have assessed that global warming rates are elevation-dependent. This so-called Elevation-Dependent Warming (EDW)—literally, the stratification of warming rates with elevation—has been assessed in different mountain regions of the globe (Pepin et al. 2015; Portner et al. 2019), often with higher rates of warming at higher elevations. Recent research has suggested that the concept of EDW should be extended to more than just temperature variations, introducing the wider concept of Elevation-Dependent Climate Change (EDCC) to better describe the elevational dependence of the changes in key climate variables encompassing several processes and mechanisms that are occurring in high-elevation environments (e.g. Kittel et al. 2002; Kuhn and Olefs 2020; Pepin et al. 2022).

Precipitation is a critical variable for mountain hydrological resources and its study is crucial in the context of climate change. Elevation is the primary factor that influences precipitation in mountainous regions. In fact, the complexity of the terrain can significantly affect local precipitation formation through orographic lifting of air masses, a phenomenon that drives condensation and cloud formation (e.g. Napoli et al. 2019). This effect leads to an increase in precipitation with elevation, commonly referred to as orographic enhancement. Such effect is modulated by the exposure of slopes to incoming atmospheric fluxes

✉ Olivia Ferguglia
olivia.ferguglia@unito.it

[1] Department of Physics, University of Turin, Turin, Italy

Published online: 26 July 2024

and to the details of the local circulation. Consequently, the analysis of elevational variations in precipitation changes becomes an assessment of whether the orographic precipitation enhancement and its modulating processes are intensifying or decreasing over time. The recent study by Pepin et al. (2022) shows that, comparing mountains to lowlands, a greatly reduced orographic gradient in precipitation temporal trends was observed globally in the recent past. Such change implies either a larger reduction of precipitation at higher elevations, or a larger increase at lower elevations, depending on the region. An average significant decrease of the precipitation orographic gradient at tropical and mid-latitudes in both hemispheres, was however accompanied by less clear results when considering individual mountain regions. Despite this general behaviour, a simple comparison of precipitation trends at high elevations against lowlands is likely not appropriately representing the actual complexity of the EDCC for precipitation, or Elevation-Dependent Precipitation Change (EDPC). Providing a general description of global EDPC is highly challenging, primarily due to the low and uneven spatial density of observational networks, and the lack of sufficiently long historical timeseries at high elevations. Moreover, data collected from traditional rain gauges are subject to systematic biases: in mountainous areas, the occurrence of snowfall (Goodison et al. 1998), the very large spatial variability of orographic precipitation, and high wind speed (Kochendorfer et al. 2017) exacerbate the challenges of reliable data collection. These limitations particularly arise when examining long-term precipitation trends and extreme precipitation characteristics. Reanalysis datasets offer a valuable compromise solution. Reanalyses combine the representation of the atmosphere-land-ocean system from state-of-the-art numerical weather prediction models with the assimilation of a wide range of observational data. Because of the numerical model, they are able to reproduce the atmospheric parameters more effectively also in regions with sparse station coverage, facilitating a more comprehensive understanding of precipitation patterns across mountainous areas. In particular, ERA5 (Hersbach et al. 2023) is a next-generation reanalysis dataset that is widely used in precipitation studies and has undergone extensive validation. Lavers et al. (2022) performed a global comparison of ERA5 precipitation and data from observations, assessing that ERA5 can be used with a high level of confidence in extratropical areas, while a lower skill was found in the Tropics, as also suggested by Valencia et al. (2023). Furthermore, ERA5 has been extensively validated in various global mountainous regions, such as the Tibetan Plateau and the Andes (Birkel et al. 2022; Sun et al. 2021).

The analysis of precipitation extremes in the context of climate change has been the focus of numerous studies, recognising their potential implications for both human societies and ecosystems (Chapter 4, SREX - IPCC, Field et al. 2012). Nevertheless, understanding changes in precipitation extremes, especially in mountainous regions, remains a substantial research challenge. The challenge of detecting long-term trends arises from the scarcity of precipitation records, particularly for the rare most extreme events, together with the high internal variability of precipitation. On the other hand, understanding their overall impact requires considering changes in atmospheric dynamics, thermodynamics, and microphysics. In mountainous regions, the increased frequency of extreme precipitation events is typically attributed to the orographic uplift mechanism, converting atmospheric moisture into precipitation, as well as thermodynamic processes intensifying extreme precipitation, driven by the Clausius-Clapeyron relationship. Additionally, various dynamical processes and precipitation formation mechanisms contribute to this phenomenon (Chapter 11, AR6 IPCC, Masson-Delmotte et al. 2021).

This study aims at comparing changes in long-term trends of mean and extreme precipitation occurrences across key mountainous areas of the globe, including the Tibetan Plateau, US Rocky Mountains, Greater Alpine Regions, and the Andes. Using the ERA5 global reanalysis dataset, we analyse the change in precipitation and its extremes from 1951 to 2020, employing selected standardised indices based on the ETCCDI definitions. The paper is structured as follows: Sect. 2 outlines the employed data and methods applied in our analysis; study areas are described in Sect. 3; Sect. 4 presents results for each mountain area individually, and Sect. 5 offers an overall joint discussion of the findings, also concluding the paper.

2 Data and methods

We have analysed daily total precipitation data provided by the fifth generation of the ECMWF reanalysis (ERA5), downloaded in October 2022 from the Copernicus Climate Change Service Climate Data Store (CDS). ERA5 is based on four-dimensional variational (4D-Var) data assimilation using Cycle 41r2 of the Integrated Forecasting System (IFS) providing records of the global atmosphere, land surface, and ocean waves. The ERA5 output is provided hourly at a 31 km horizontal resolution, then post-processed to obtain daily precipitation totals and interpolated onto a $0.25° \times 0.25°$ latitude-longitude regular grid. The adopted total precipitation parameter includes both liquid and frozen water, i.e. rain and snow, accumulated at the Earth's surface. Precipitation is modelled by IFS through its cloud scheme, which reproduces the occurrence of stratiform clouds and large-scale precipitation at grid scales, or larger, based on cloud microphysical processes at the given atmospheric conditions (e.g., pressure, temperature and moisture), and by the convection scheme, producing convective precipitation

at sub-grid scales. Since convection is considered at sub-grid scale, convective precipitation falls immediately to the ground, contrary to large-scale hydrometeors, which get advected by the wind. Although IFS does not assimilate directly rain-gauge observations, the model is aided by assimilation of composite radar/rain-gauge precipitation estimates since 2009. More information about the ERA5 dataset can be found in Hersbach et al. (2023).

We considered mean precipitation (**Pm**) and its variance together with a selection of precipitation indices from the ETCCDI project (Karl et al. 1999) to describe different aspects of precipitation. We include indices ranging from heavy and very heavy precipitation, typically regarded as moderate extremes, to severe extremes. The indices of extremes are synthesised in the following list:

1. **R10mm** Annual count of days with heavy precipitation, i.e. when precipitation exceeds the threshold of 10 mm/day [*days*]
2. **R20mm** Annual count of days with very heavy precipitation, i.e. when precipitation exceeds the threshold of 20 mm/day [*days*]
3. **Rx1day** Annual maximum 1-day precipitation [*mm/day*]
4. **R95p** Annual total precipitation exceeding the 95th percentile threshold on wet days evaluated over the 1961–1990 reference period [*mm/year*]
5. **CWD** Annual maximum length of wet spell: maximum number of consecutive rainy days [*days*]
6. **CDD** Annual maximum length of dry spell: maximum number of consecutive dry days [*days*]

A wet day was assumed as a day with precipitation above 1 mm. Indices were calculated yearly for the period 1951–2020 at individual grid points, and then averaged as needed. The elevational dependency of precipitation changes was studied through two complementary approaches applied to the selected precipitation indices.

First, trends in precipitation indices over the period 1951–2020 were calculated for individual grid points within each study area. The existence of an EDPC signal was assessed using a least squares estimate of the linear regression of elevation vs. trend values, testing its significance at 95% level (for computation details and formulas please refer to Storch and Zwiers (Chapter 8, 1999). Additionally, the reduced chi-squared analysis was applied to determine whether a simple linear regression adequately describes the distribution's behaviour (Chapter 6, Storch and Zwiers 1999). This analysis was complemented by an examination of geographical maps of trends to investigate the influence of different geographic factors.

As a second approach, each study area was divided into 500 ms-high elevational bins, and each precipitation index was spatially averaged within each bin. The width of each bin was set by requiring that at least 10 grid points fall within it. Temporal trends were evaluated with a linear regression from 1951 to 2020 for timeseries in each bin, accepting a statistical significance at the 95% confidence level. Trends were then compared at various elevations to identify positive (or negative) elevational gradients. Following other studies on EDW focused on different areas (e.g. Palazzi et al. 2019), in this study only grid cells with elevation above 500 m a.s.l. were kept in the calculation of vertical gradients, although these areas are shown in the plots to facilitate comparisons and considerations.

To investigate particular cases, transects were extracted across mountain chains to discern the effects of elevation beyond geographical variability. Transects were considered either along the meridional or zonal direction, depending on the main direction of the mountain chain, and built averaging three adjacent longitude or latitude grid points across the transect. They were further used to differentiate west-east or south-north variations in the elevational dependency of the trends, due to the likely different climatic regimes affecting the two sides of a mountain chains (e.g. Toledo et al. 2022).

3 Mountain areas

Elevational patterns of precipitation change were studied over four main mountain areas of the world, i.e. the Tibetan Plateau (TP, 60°–120°E; 18°–47°N), the Greater Alpine Region (GAR, 4°–19°E, 43°–49°N), the Rocky Mountains (RO, 235°–265°E, 30°–50°N) and the Andes, the latter subdivided into their tropical - Northern Andes (ANN, 280°–300°E, -23°–0°N) and mid-latitude parts - Southern Andes (ANS, 280°–300°E, -40°– -23°N). The study areas, contoured by the violet rectangles, are displayed in Fig. 1 where their climatological precipitation (average in the period 1951–2020) in boreal summer months (from June to September, panel a) and boreal winter months (December to March, panel b) is also shown.

Besides being among the largest mountain regions in the world, the selected areas are representative of tropical and middle latitudes, monsoon and large-scale circulations, and a variety of regional influences. TP, GAR and RO are in the northern mid-latitudes, all exposed to westerly circulation, with the TP largely affected by the monsoon circulation, and the latter two by cyclonic activity and local summer convection. The Andes stretch over the tropics and mid-latitudes, and are only marginally affected by westerly circulation, with most precipitation coming from the east. The area of the tropical Northern Andes is reached by the InterTropical Convergence Zone (ITCZ) while the southern part is exposed to an alternation of local dry winter and wet summer. The RO and the Andes share a preferential meridional orientation along the

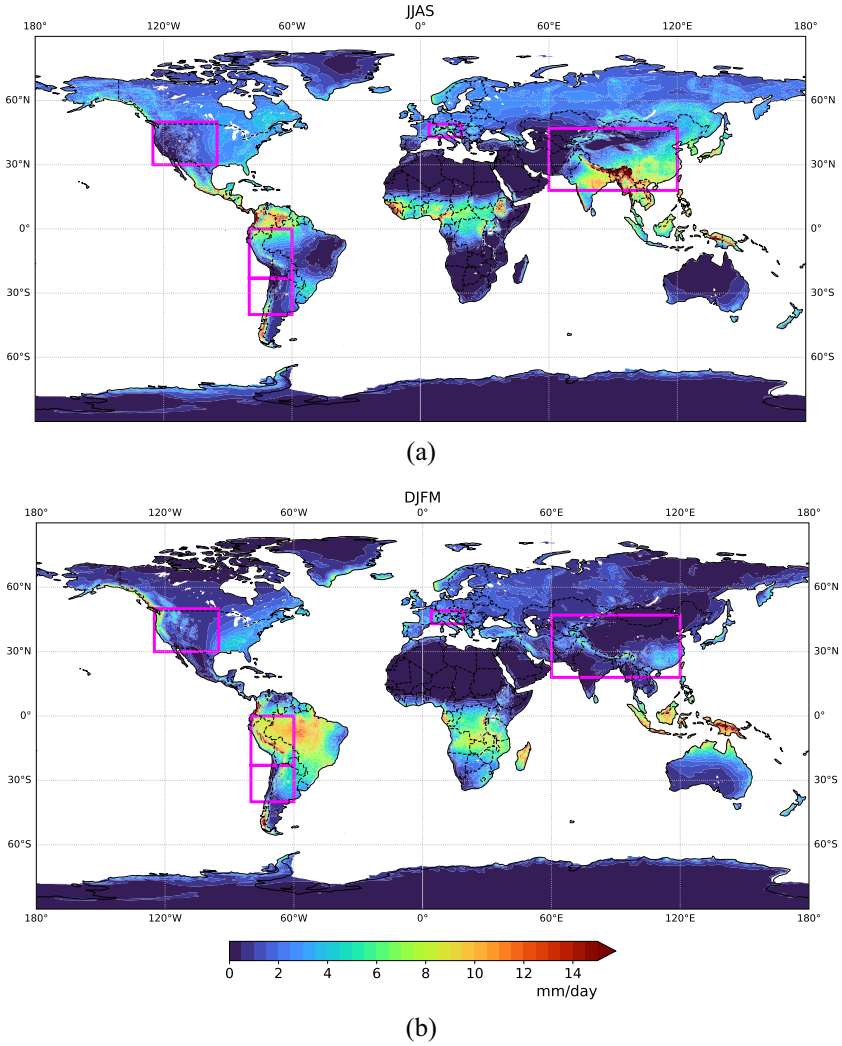

Fig. 1 Climatology map of precipitation in *mm/days* (1951–2020) with the definition of the mountain areas considered in this study for the extended boreal summer (JJAS, panel **a**) and winter (DJFM, panel **b**)

Pacific Ocean, whereas the GAR and the Himalayas within the TP have largely a zonal orientation. Further regional characteristics are discussed in the following sections.

3.1 The Tibetan Plateau

Figure 2 shows the orography map of the Tibetan Plateau (TP, panel a), and the elevation profiles at three reference transects highlighted in panel a (panel b). Additionally, a

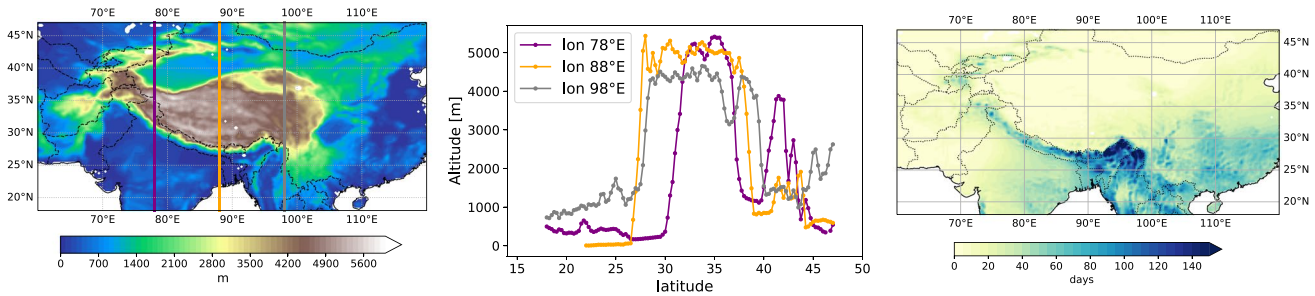

Fig. 2 Orography [m a.s.l.] of the Tibetan Plateau region (**a**); elevation profiles along the three transects highlighted in panel a (**b**); map of heavy precipitation (R10mm index, in days/year) averaged over the 1951–2020 period (**c**)

map of the geographical distribution of the R10mm index averaged over the period 1951–2020 is shown to describe heavy (or moderate extreme) precipitation across the region (panel c). The TP, often referred to as the "Third Pole" of our planet, stands as the world's largest and highest plateau, serving as a water source for the majority of rivers that supply vital water resources to the population of south and east Asia (Immerzeel 2020). In the recent decades, the TP has undergone significant warming (Bibi et al. 2018; Yao et al. 2016) with rates of temperature increase exhibiting an elevational-dependency, being more pronounced at higher compared to lower elevations (e.g. Liu et al. 2009). Furthermore, an increase in moisture content and precipitation across the TP has been identified in recent decades (Yang et al. 2011). In this area, precipitation is characterised by large spatial variability, varying throughout different locations on the Plateau (Bibi et al. 2018), with the largest amounts concentrated at the southern edge of the Plateau both in terms of total precipitation (see Fig. 1) and its extremes (Fig. 2c). Two main sub-regions can be distinguished, depending on their exposure to the influence of different atmospheric circulation patterns (e.g. Palazzi et al. 2013): The eastern Himalayan region receives the majority of precipitation and exhibits the largest number of intense rainy days, as illustrated in Fig. 2c. This pattern is primarily shaped by the dynamics of the summer monsoon: The northward movement of moisture from the Indian Ocean, driven by the Southwest Indian monsoon causes a prevalence of rainfall occurring in the summer season, typically from June to September, as shown in Fig. 1a (Li and Yanai 1996; Krishnamurti and Kishtawal 2000; Palazzi et al. 2013). On the western side, in the Hindu-Kush Karakoram region, precipitation is observed mainly in the winter months (Fig. 1b), primarily due to the influence of western weather patterns, also referred to as Western Disturbances, that carry moisture from the Atlantic region, the Mediterranean and Caspian Sea (Singh and Kumar 1995; Archer and Fowler 2004; Syed et al. 2006; Treydte et al. 2006; Midhuna et al. 2020). It is also worth highlighting that the entire TP region has been the subject of numerous regional and local studies analysing specific aspects of precipitation patterns, such as the transitioning from solid to liquid precipitation at mid and high elevations in the Sikkim Himalaya (Kumar and Sharma 2023) or changes in extreme precipitation in the Uttarakhand Himalaya (Kumar et al. 2024).

3.2 The Greater Alpine Region

Figure 3 shows the orography map of the Greater Alpine Region (GAR, panel a), elevation profiles along the three meridional reference transects (panel b), and the geographical distribution of the R10mm index over the period 1951–2020.

The GAR is a particularly interesting geographical area: One of the highest and largest European mountain chains, it is sensitive to different atmospheric synoptic regimes, mainly originating from the Atlantic and the Mediterranean Sea. Besides seasonal differences, precipitation patterns are influenced by several factors including orography. These patterns exhibit substantial inter-annual variability and are also subject to the influence of larger atmospheric patterns, such as the North Atlantic Oscillation (NAO) or El Niño Southern Oscillation (ENSO). A comprehensive exploration of these regional climate characteristics can be found in the detailed study by Schär et al. (1998). The GAR is geographically positioned between two distinct climatic zones—the mid-latitude temperate climate and the Mediterranean climate type—which are experiencing, and are projected to experience, opposite increasing (central Europe) and decreasing (Southern Europe) precipitation trends. Consequently, the alpine precipitation patterns exhibit notable spatial variations, both in terms of long-term average precipitation and intensity and frequency of extreme events. Nonetheless, total precipitation generally tends to increase with increasing elevation, although the relationship between elevation and precipitation displays significant variability depending on the location and season (Schär et al. 1998). Heavy precipitation also displays a dependence on the elevation, reaching

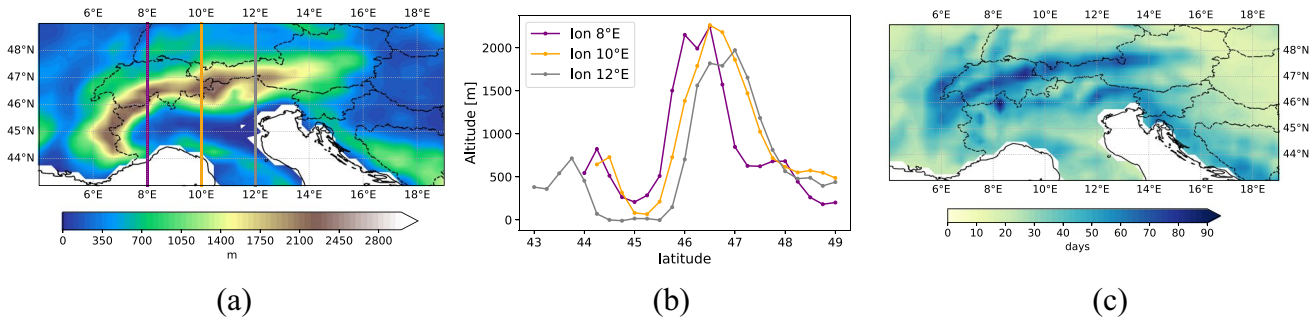

Fig. 3 Orography [m a.s.l.] of the Greater Alpine region (**a**); elevation profiles along the three transects highlighted in panel a (**b**); map of heavy precipitation (R10mm index, *days/year*) averaged over the 1951–2020 period (**c**)

its maximum on the northern side of the mountain chain, as evident from Fig. 3c. Moreover, the seasonal cycle of heavy precipitation exhibits notable geographical variability: The northeast area shows a defined single peak during summer, whereas the northwest area experiences a second one, albeit weaker, during winter. The most intense precipitation is usually observed during summer months, generally associated with convective weather systems (Schär et al. 1998).

3.3 The US Rocky Mountains

Figure 4 shows the orography map of the US Rockies (RO, panel a), elevational profiles along the three meridional reference transects highlighted in panel a (panel b), and the geographical distribution of the R10mm index over the period 1951–2020. Both mean precipitation (Fig. 1) and heavy precipitation (Fig. 4c) show considerable spatial variability in the area with the highest R10mm values localised in the northern coastal area, influenced by the influx of cool and moist air from the northern Pacific Ocean. The complex topography strongly influences the distribution of precipitation over the mountainous regions, giving rise to a classic orographic precipitation pattern characterised by enhanced rainfall on the windward side and a rain shadow on the lee side of the mountain (Kittel et al. 2002). This effect is maximised in the winter seasons, as shown in Fig. 1b. During the summer season, the northern coastal areas is characterised by intense precipitation, whereas the south-west of the RO experiences dry condition due to the impact of dry continental air and monsoonal flows from the Gulf of Mexico and California (Kittel et al. 2002).

3.4 The Andes

Figure 5 shows the orography of the Andes (AN, panel a), together with the map of the geographical distribution of the R10mm index (panel b).

The AN mountain chain represents the predominant topographical feature of South America, stretching 7000 kms, from the Tropics to mid-latitudes, which leads to high spatial variability of precipitation fields. Given the influence of the tropics and extra-tropics, the region was divided into two distinct areas: The Tropical Andes in the North (ANN), characterised by higher precipitation, and the Subtropical Andes (ANS) in the south, prone to by drier conditions, in accordance with the geographical analysis performed by Toledo et al. (2022).

The ANN serves as a natural barrier separating the persistently humid Amazon Basin air to the east from the arid Pacific coast air to the west. This distinction can be noticed also in heavy precipitation patterns shown in Fig. 5b. Climate in this region can be characterised by relatively dry conditions in austral winter season (JJAS), and wet conditions during the austral summer (DJFM) (see mean precipitation in Fig. 1). During the central austral winter months (June-August) in fact, the subtropical jet stream reaches its northernmost position, creating a block for the moisture transport from the Amazon region, leading to a dry climate (Potter et al. 2023). During austral summer, the jet stream weakens and shifts southward allowing the eastern side of the Cordillera to serve as a convergence point for atmospheric moisture originating from both the ITCZ and the South American Monsoon System (SAMS), causing extremely wet conditions, with the most intense rainfall concentrated near the summit of the chain (Caicedo et al. 2020), as can be notice in Fig. 5b.

The ANS exhibits a distinct seasonal geographical pattern. Specifically, during the local winter season, the ANS (south of 30°S, the last part of the mountain chain) features a dry east side and a wet west side of the chain. This is attributed to a predominant atmospheric moisture source originating from the evaporation over the Pacific Ocean (Gimeno et al. 2016). In contrast, during the local summer (DJFM), precipitation in the ANS concentrates on the eastern side

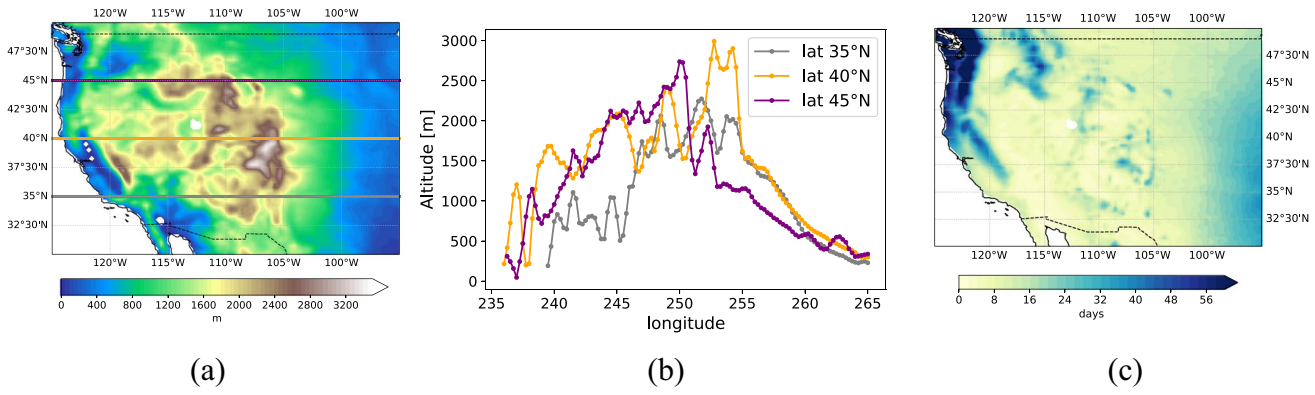

Fig. 4 Orography [m a.s.l.] of the Greater Alpine region (**a**); elevation profiles along the three transects highlighted in panel a (**b**); map of heavy precipitation (R10mm index, *days/year*) averaged over the 1951–2020 period (**c**)

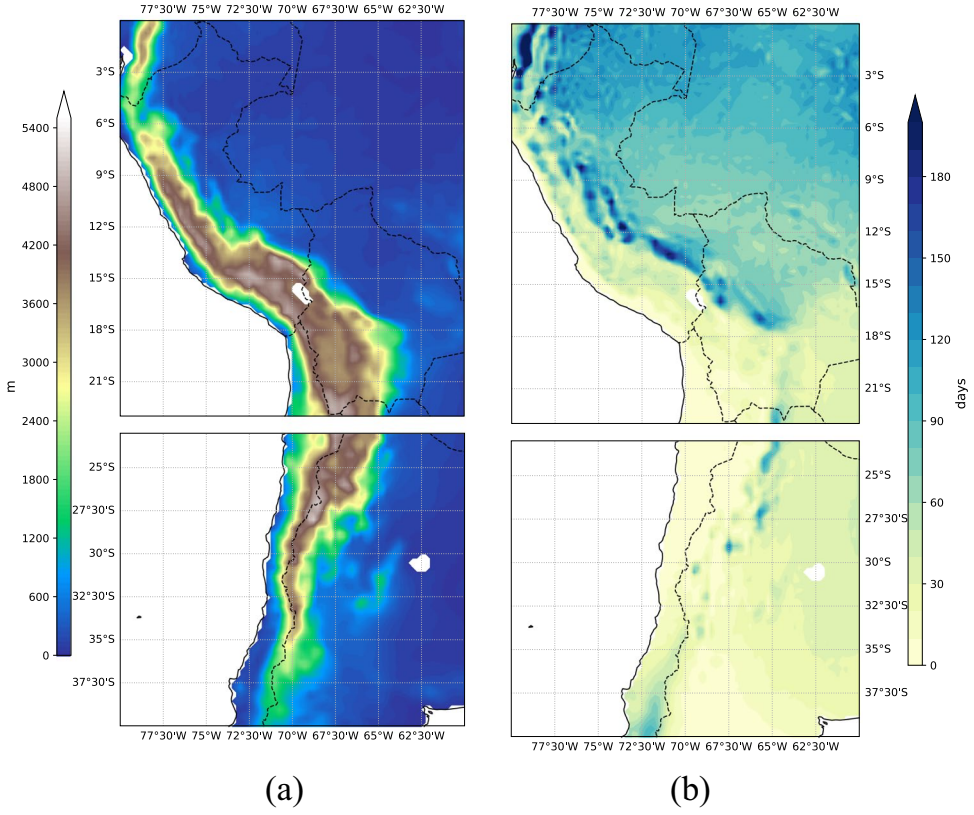

Fig. 5 Orography [m a.s.l.] of the tropical and Sub-tropical Andes (ANN, ANS, panel **a**) and a map of the geographical distribution of heavy precipitation (R10mm index, days/year) evaluated over the 1951–2020 period (**b**)

of the chain, while the western side experiences minimal rainfall (Caicedo et al. 2020).

4 Results

The elevational dependency of ERA5 trends in mean precipitation and extreme precipitation indices was studied with the methodology described in Sect. 2. Table 1 summarises the results obtained evaluating the value of the elevational gradient, computed as the linear regression of the distribution of elevations versus trend values at all grid points in each study region (approach 1, as explained in Sect. 2).

In the TP, GAR and ANS, a significant positive elevational gradient is found in both mean and heavy precipitation (R10mm) trends, further extending to the maximum yearly duration of consecutive wet days (CWD). On the contrary, the RO region exhibits an opposing sign, with consistent negative vertical gradients in the trends of all indices but CDD. The ANN shows no clear vertical gradients of trends. The chi-squared analysis suggests that for TP and ANS, a simple linear regression may not be the most appropriate method to describe the elevational stratification, as a more complex vertical pattern may be present. Remarkably, each mountain region, except ANN, consistently shows a similar behaviour in terms of the vertical gradient of change in several indices, except for consecutive dry days (CDD), which exhibits an opposite gradient in both the ANS and RO. Another exception is represented by the GAR, where only mean precipitation (Pm), heavy precipitation (R10mm),

Table 1 Summary of the elevational dependency of ERA5 precipitation indices trend over each region: Tibetan Plateau (TP), Greater Alpine Region (GAR), Rockies (RO) and Andes (AN) divided into the Northern part (ANN) and the Southern part (ANS). Orange (blue) colour refers to a positive (negative) elevational gradient evaluated at the 95% confidence level

	Pm	R10mm	R20mm	Rx1day	R95p	CWD	CDD
TP							
GAR	*	*				*	
RO	*	*	*	*	*	*	*
ANN							
ANS				*			

The asterisk implies an acceptable reduced chi squared analysis (minor than 2). Empty cells indicate either no clear or no significant correlation

and the maximum yearly duration of consecutive wet days (CWD) exhibit the same EDPC signal.

The methodology, which is extensively used in the literature, leads to shortages in interpreting the results. In fact, a positive (or negative) gradient can be the result of various phenomena occurring at both high and low elevations. For example, a positive elevational gradient in precipitation indices can be attributed to one out of three scenarios: 1) A more pronounced increase in precipitation (wetting) at higher elevations compared to the increase at lower elevation; 2) a larger reduction in precipitation (drying) at lower elevation compared to that at higher elevations, or 3) a contrast between wetter conditions at higher elevations and drier conditions at lower elevations. Therefore, the adoption of a complementary methodology becomes essential. As already explained in Sect. 2, the study areas were subdivided into elevational bins of 500 ms width, and the temporal trends were computed within each bin, considering also their related errors and statistical significance (p-value) to critically analyse the vertical profile. Additional insights into the unique characteristics of each mountain region are detailed in subsequent sections.

4.1 The Tibetan Plateau

Figure 6 shows the details of the vertical profile of ERA5 temporal trends of spatially averaged binned data superimposed to the distribution of trends at individual grid points over the region. Most individual trends tend to cluster, leading to largely compact distributions, especially at higher elevations where the number of points is smaller, and the influence of the lowlands is damped. Deviations from the core of the distribution are more pronounced towards smaller values of the indices below 2000 ms, and towards higher values above, contributing to increasing the steepness of the vertical gradient and a larger positive change in extreme precipitation at higher elevation. As summarised in Table 1, all indices in the Tibetan Plateau show an overall positive vertical gradient of temporal trends from 1951 to 2020, except CDD. Trends of Pm (panel a), R10mm (panel b), and CWD (panel c) exhibit a consistent behaviour: Profiles show a positive gradient up to about 4000 ms, where an inversion occurs. Significant negative trends below 2000 ms indicate a drying effect that decreases with the elevation. On the contrary, the significant positive trend from around 4000 ms

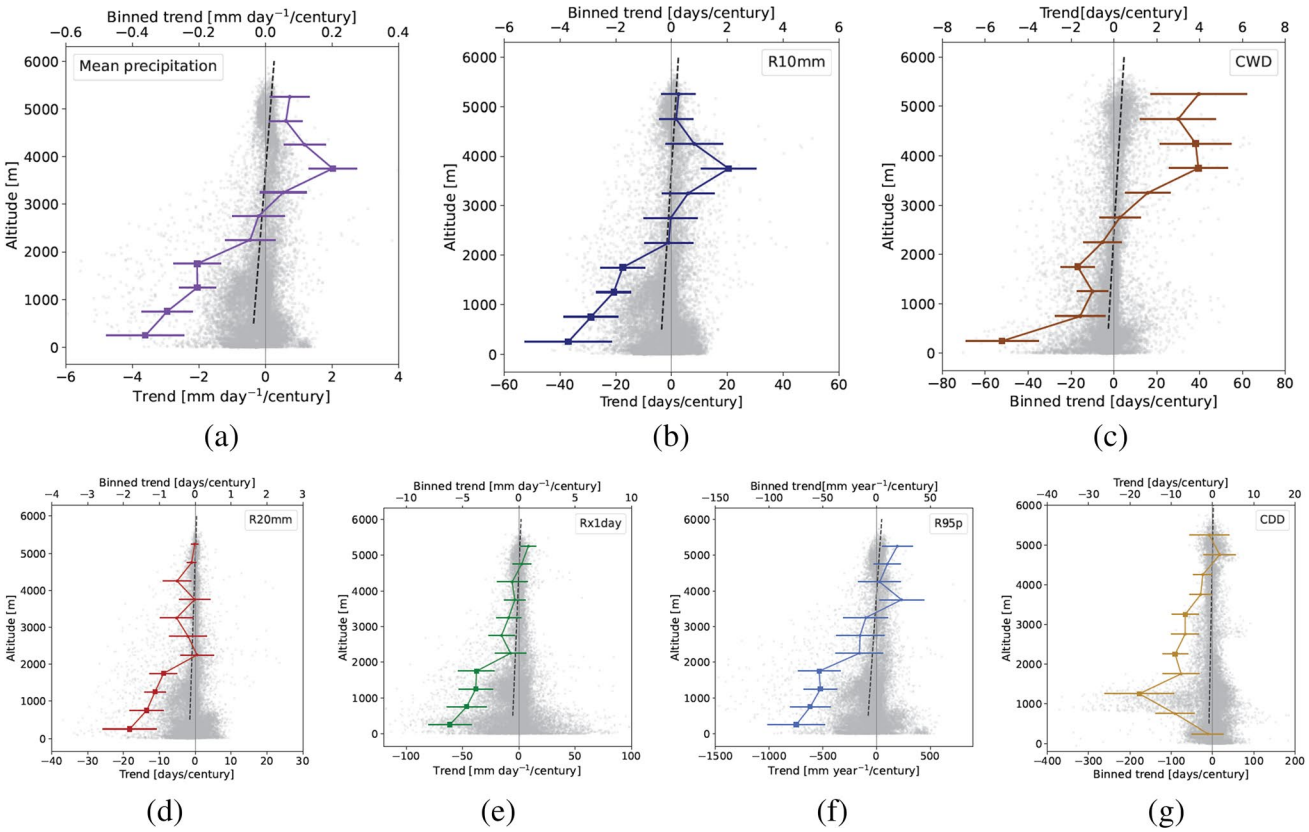

Fig. 6 Elevational dependence of temporal trends of ERA5 precipitation indices (see labels). Each panel shows the vertical profile of spatially averaged binned data (top scale) superimposed to the distribution of trends at individual grid points (grey, bottom scale) over the Tibetan Plateau. Vertical profiles include errors on the trend and the significance of the trend (filled squares when >95%). Point distributions are accompanied by their linear regression (dashed line). Please note that the scale for vertical profiles is magnified by a factor 10

indicates increased wetting effects at very high elevations. Trends of R20mm (panel d), Rx1day (panel e), and R95p (panel f) show an overall positive gradient with elevation, with a change in the slope around 2000 ms. As described for the other indices, the significant negative trends below this threshold indicate a drying signal at low elevations, which decreases with elevation. Trends of CDD has a broad distribution between about 500 and 2000 ms likely due to the presence of areas characterised by very distinct microclimatic conditions (e.g. the Taklamakan desert). Above this elevational threshold, changes of CDD are characterised by an overall positive elevational gradient and significant negative trends around 1000 ms, indicating a higher persistence of drought conditions.

The impact of geographical variability was investigated by inspecting maps of trends and the elevational dependency (see Fig. 7) along the three meridional transects already introduced in Fig. 2. Transects clearly reveal how geographical differences impact on the vertical distributions: The northern region exhibits limited elevational stratification, whereas the southern area displays a "knee-shaped" vertical profile. Precipitation decreases progressively up to 2000 ms; at this level an inversion occurs, and negative trends increase toward zero. Furthermore, the 98° latitude transect highlights the high-elevation wetting effect also found in the vertical profile of binned data (Fig. 6).

4.2 The Greater Alpine Region

Figure 8 describes the vertical profile of the indices trend over the GAR, for both binned data and the grid-points distribution. In both cases, trends of Pm (panel a), R10mm (panel b) and CWD (panel c) show clear linear positive elevational gradients. They indicate an enhancement of precipitation trend with elevation and consequently a significant wetting signal at high elevations (above 1000 ms). The other indices show no clear elevational stratification of their temporal trends.

An investigation of the R10mm trend map and the vertical profile of the three meridional transects was performed (Fig. 9). An evident discontinuity can be seen between positive trends in the northern side and negative trends in the southern side of the region. Even though this difference leads to a bias between the southern and northern branches of the distribution of trends along the transects, the elevational-gradient of the two distributions exhibit the same sign. The positive elevational dependency in the GAR is therefore robust and independent on geographical variations.

4.3 The US Rocky Mountains

The Rocky mountains show an opposite sign of the elevational gradient compared to the previous regions, both in the distributions and in the vertical profiles (Fig. 10). Once again, trends of Pm (panel a), R10mm (panel b) and CWD (panel c) show the clearest elevational dependency, with increasingly larger reductions at higher elevations, confirming the enhanced drying at higher elevations obtained with the first method. The same pattern can be identified in the other indices, except for CDD, which exhibits an opposing gradient, even though no significant trends can be seen in the binned data. All indices trends (except CWD) are characterised by a broad and non-homogeneous distribution, presenting a negative tale below 2000 ms. Inspection of vertical distributions along transects shows that this deviation from the compact bulk of the distributions is due to the geographical variability in the region (see results for transect at 45°N, Fig. 11). The northern coastal area, characterised by low elevations, has in fact experienced a strong reduction in both mean and extreme precipitation over the past decades, therefore leading to the broadening of the distribution.

Figure 11 shows the vertical profiles of the three zonal transects described in section 3.3. They exhibit two very

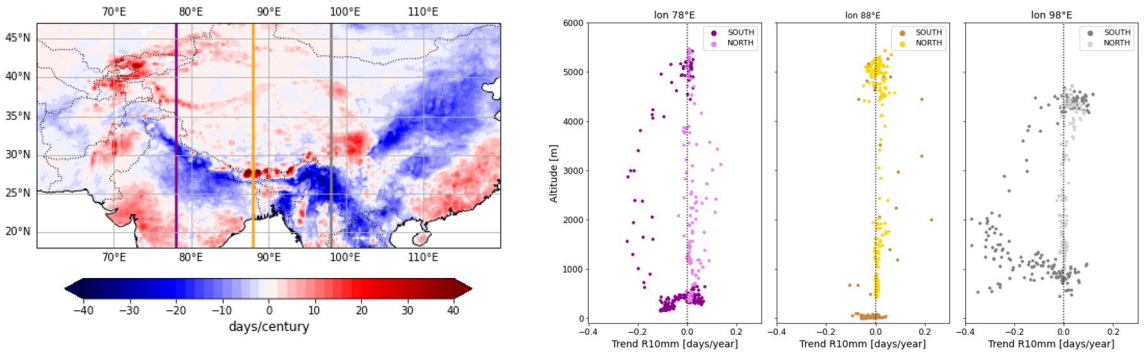

Fig. 7 Geographical distribution of trends in heavy precipitation (R10mm) over the 1951–2020 period (left) and their elevational distribution (right) along the three meridional transects defined in Fig. 1 and reported on the map as colour-coded vertical lines. Grid points were separated in northern and southern parts assuming the maximum elevation along the transect as separator

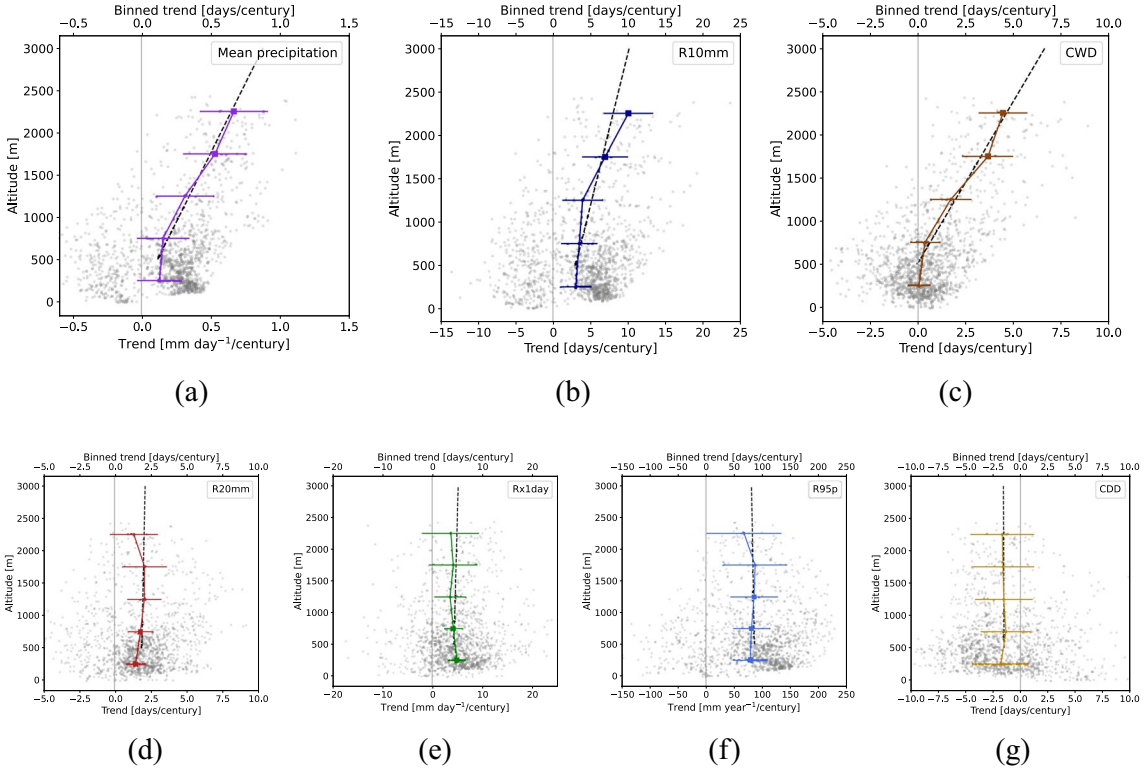

Fig. 8 As in Fig. 6 but for the GAR

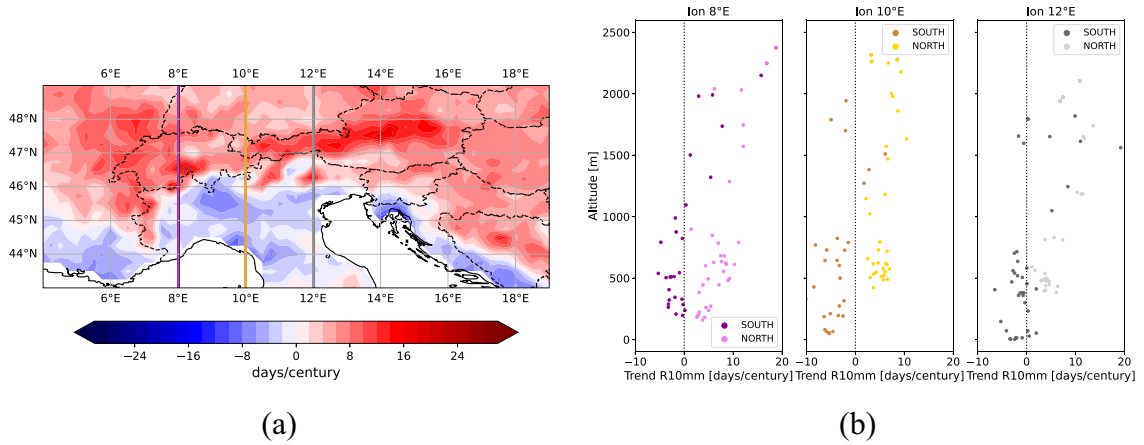

Fig. 9 Geographical distribution of trends in heavy precipitation index (R10mm) over the 1951–2020 period (**a**) and their elevational distribution (**b**) along the three meridional transects reported on the map as colour-coded vertical lines. Grid points were separated in northern and southern parts assuming the maximum elevation along the transect as separator

distinct patterns up to 1500 to 2500 ms depending on the latitude, with much lower values in the western slopes. Such biases affect vertical gradients together with a large contribution to the variance and branching in the overall distributions. The elevational distribution shows a clearly different behaviour separating the western and the eastern side of the chain, especially at low and mid-elevation. The two sides reconcile at higher elevation.

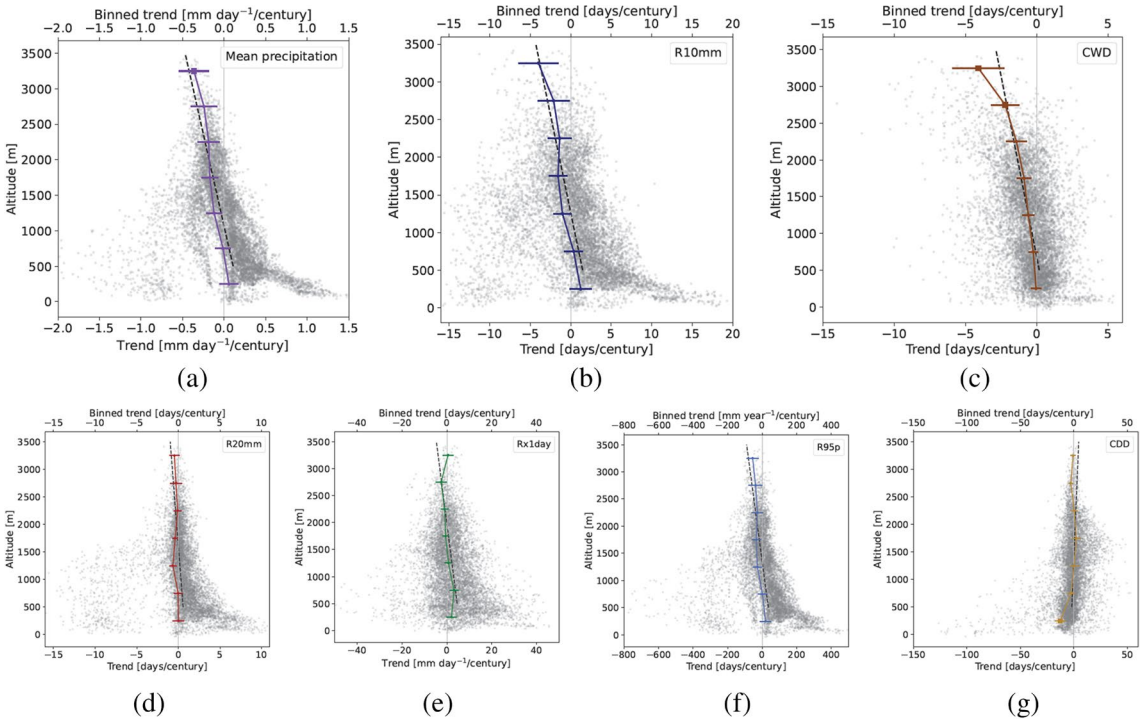

Fig. 10 As in Fig. 6 but for the RO

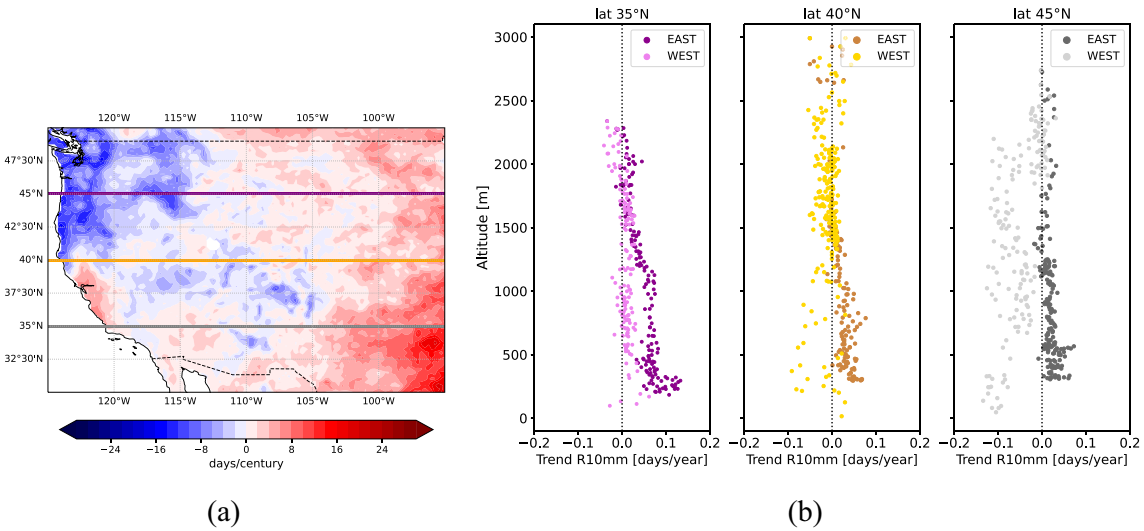

Fig. 11 As in Fig. 9 but for the RO

4.4 The Andes

Figure 12 shows the vertical profile of the binned data over the Andes, both tropical and subtropical, for Pm (panel a,d), R10mm (panel b,e) and CWD (panel c,f). As for the other mountain areas, trends Pm, R10mm and CWD exhibit similar patterns and align with the other indices shown in Figures S1 and S2 in the Supplementary Information (SI). Two clearly distinct behaviors can be identified in the tropical and sub-tropical regions. Generally, the ANN exhibits no elevational stratification while the ANS profile shows a more complex dependency with the elevation. The latter is characterised by two different gradients with opposite sign, showing a knee-type curve with an inversion around 2000 ms. Below 4000 ms, the ANS profile is characterised by negative trends, revealing a drying effect in both mean

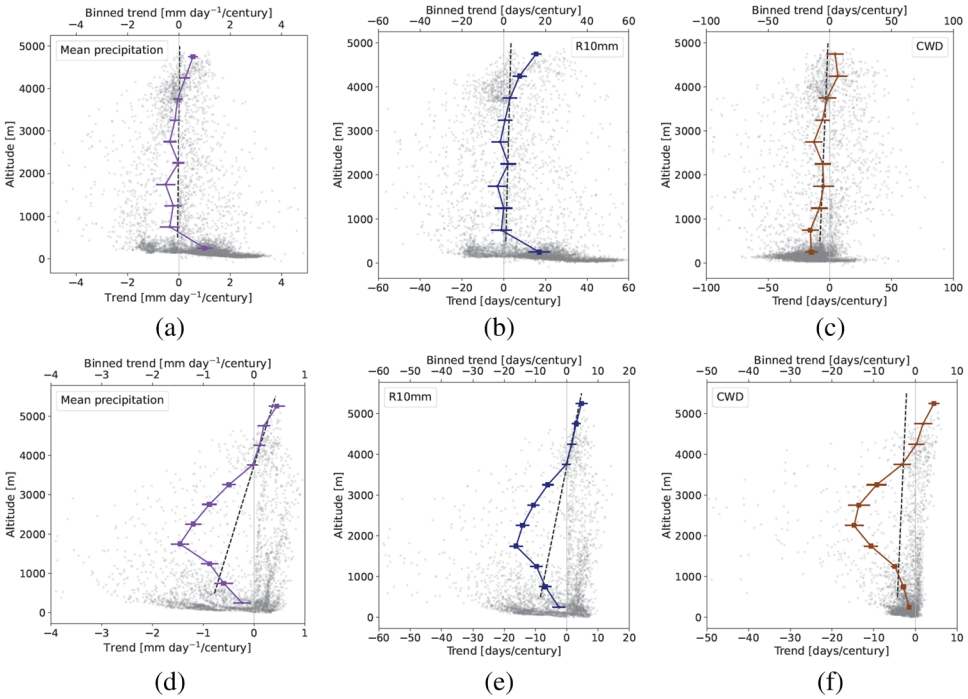

Fig. 12 As in Fig. 6 but for the Andes tropical (above) and subtropical (below)

and extreme precipitation. This holds the results obtained with the first method, that is, a simple linear regression might not be sufficient to describe the real elevational dependency. Nevertheless, the ANN and the ANS share certain common characteristics. Primarily, above 4000 ms, both regions exhibit a positive elevational gradient with positive trends, highlighting a wetting phenomenon occurring at very high elevations, similarly to what has been assessed in the TP and GAR regions. Furthermore, both distributions are notably broad, particularly at mid- and low- elevations, making an examination of the trends geographical variability necessary. Taking the driving precipitation mechanisms into account, it is crucial to examine the western and eastern sides of the mountain chain separately. In this case, performing a zonal transect analysis is not convenient owing to the narrow extent of the Andes, resulting in a limited number of grid points within a single transect. Consequently, the entire area has been considered averaging the eastern and western side of the chain separately.

Figure 13 shows the vertical profile of binned data of R10mm, dividing the western and the eastern side of the chain. The broadness of the overall distribution, shown in Fig. 12 (panels a and e), can be ascribed to the large differences in elevational profiles of trends between the eastern

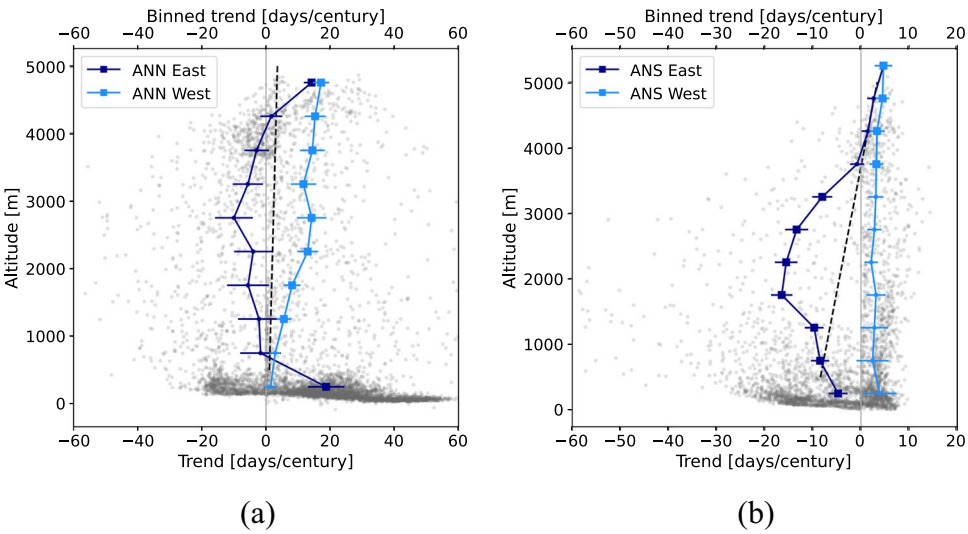

Fig. 13 Elevational dependence of ERA5 temporal trends of R10mm for the tropical (**a**) and subtropical (**b**) Andes, dividing eastern and western side of the mountain chain. The plot shows the vertical profile of spatially averaged binned data (top scale) of east (blue) and west (light blue) side of the chain superimposed to the distribution of trends at individual grid points (grey, bottom scale). Vertical profiles include errors on the trend and the significance of the trend (filled squares when >95%)

and western side of the mountain chain. The west side has a similar profile in both tropical and sub-tropical Andes: Trends are positive, showing significant enhanced precipitation changes at higher elevations. The overall profiles show a positive elevational gradient for the ANN while no significant signal can be assessed in the ANS. On the contrary, the eastern side of the ANN has no significant vertical gradient and above 4000 ms its behaviour becomes consistent with the eastern side. In the ANS, the overall profile is dominated by the behaviour of the the eastern side, which shows the peculiar knee-shape at mid-elevations, shown in Fig. 12 (panel d, e and f).

5 Discussion and conclusions

The relevance of an elevational dependency of climate change is tied to a vertical stratification of patterns of change, which is shared by mountains around the globe beyond their regional differences. This has been explored in the literature largely in terms of temperature trends (EDW), typically assessing the vertical gradient of temporal trends against elevation calculated over individual grid points in a region, or examining the vertical profile of elevational-binned spatially averaged trends. In this paper we applied two complementary methodologies to precipitation and precipitation extremes ERA5 indices to explore the elevational dependence of their trends in four mountain regions of the world and identify the dominant effect (either drying or wetting) responsible for the elevational gradient.

In the Tibetan Plateau, all indices show a positive elevational gradient of precipitation changes, with a significant reduction of precipitation and its extremes at lower (compared to higher) elevation. The evaluation of the binned profiles revealed that all indices consistently exhibit a drying effect at low elevations, especially below 2000 ms, that is attributable to the behaviour found in the southern part of the Tibetan Plateau as highlighted by the transect analysis. Moreover, mean precipitation (Pm), heavy precipitation (R10mm) and the length of consecutive wet days (CWD) show a significant wetting signal above 4000 ms, a feature shared by both sides of the chain. This result is consistent with Hu et al. (2021) who used data from 113 meteorological stations along the period spanning from 1971 to 2017. In their study, the authors identified a positive stratification with elevation for total precipitation, R10mm, and CWD, labelling this phenomenon Elevation-Dependent WEtting (EDWE). EDWE was assessed using in-situ observations also in the central arid region of China (Yao et al. 2016) and during the summer season over the Tibetan Plateau (Li et al. 2017), highlighting a growing body of evidence indicating an intensified wetting at higher elevations. The robustness of the wetting effect is also supported by an intercomparison analysis we conducted for the elevational gradient of trends in annual total precipitation using the two observational datasets GPCC and CRU. The complete results of the analysis over all mountain regions considered are reported in the Supplementary Information (SI). When considering the winter and summer seasons separately, this phenomenon emerges to be primarily attributable to the summer months. The drying effect may be explained in terms of circulation changes, in particular by the recent warming-driven weakening of the Indian summer monsoon (Kumar et al. 2020). A weakening of the South Asian monsoon circulation was shown to drive the decline in seasonal average rainfall over northern India and southwestern China from the 1950 s to the early 2000 s (AR6, IPCC, Masson-Delmotte et al. 2021). Besides the warming effect (Kumar et al. 2020), this decline has been associated with the impact of local aerosol emissions, which saw a dramatic increase due to the rapid industrialization of the region land use/cover change (Paul et al. 2016) and reduced temperature gradient (thermal contrast) between Indian Ocean and northern land mass (Tibetan Plateau) (Mukherjee et al. 2015; Yadav et al. 2024).

In the Greater Alpine Region, ERA5 Pm, R10mm, and CWD trends exhibit a positive gradient with elevation, and this is consistently found using both employed methods (the vertical gradient of the overall distribution and the binned vertical profile). Such behaviour is partially found also in GPCC annual total precipitation (see SI). This stratification highlights a wetting signal above 1500 ms. As for the Tibetan Plateau, we found the wetting signal been driven by exclusively the summer season behaviour. The positive vertical gradients is shared by both the northern and southern sides of the chain, though with a bias in the absolute values, suggesting the drivers to be consistent on both sides. Trends for the further precipitation indices do not exhibit any clear elevational dependency. Elevational patterns in the GAR were examined in terms of future projections of both mean and extreme precipitation in previous studies (e.g. Kotlarski et al. 2012; Gobiet et al. 2014; Napoli et al. 2023). These studies showed that changes in summer precipitation in the GAR are significantly influenced by elevation, showing a positive gradient primarily due to a notable drying effect at lower elevations. Moreover, another study (Giorgi et al. 2016) found out that high-resolution regional climate models (around 12 km of spatial resolution) show an increase in mean and extreme precipitation trends over the high-altitude Alpine areas, a signal not seen by global and coarser simulations. In the historical period considered in this study and in the GAR, ERA5 seems to capture the convective signal associated with the summer precipitation pattern, although other studies analysing convective precipitation globally suggest the importance of using higher resolution datasets to capture small-scale processes such as summer convection (Capecchi et al. 2022) and ERA5 capability in accurately

estimating convective precipitation (Lavers et al. 2022). In contrast, Gobiet et al. (2014) identified a negative elevational gradient in total winter precipitation. They attributed the gradient to changes in convection, possibly resulting from thermodynamic processes, and the influence of the positive (or warm) phase of the North Atlantic Oscillation on winter precipitation changes, a classification that we did not introduce in our analysis.

Somehow surprisingly, the EDPC calculated with ERA5 in the US Rocky Mountains exhibits an opposite behaviour compared to the other regions: all precipitation trend indices show a consistent and significant negative vertical gradient, primarily due to a pronounced drying effect at high elevations, particularly above 2500 ms. At lower elevations, the western and eastern sides of the mountain chain exhibit an opposite elevational gradient. This effect can be attributed to the strong precipitation decrease that characterises the northwest coastal area, as detailed by the transect analysis. Despite the clarity of these results in ERA5, significant differences have been identified in the binned elevational profiles of annual total precipitation trends in CRU and GPCC datasets (see SI). This aligns partially with the findings of Pepin et al. (2022) who examined regional precipitation changes across global mountains compared to lowlands, using different datasets (CRU, GPCC, ERA5 and CMIP5 models). In fact, they also found a negative gradient with the elevation, which was significant only in CMIP5 models.

In both the tropical and subtropical Andes, the elevational stratification of ERA5 temporal trend of precipitation indices can not be described by a simple linear regression. In the tropical zone, no discernible elevational dependency was identified. The subtropical zone, on the contrary, displays a more complex vertical pattern, characterised by a linear vertical profile in the west of the mountain chain, and a "knee-shaped" profile in the east, with a negative vertical gradient below about 2000 ms and positive gradient above. Further analysis revealed that throughout the entire Andes, the annual profile on both sides of the chain is predominantly influenced by the summer (DJFM) signal. Particularly, in the tropical Andes (ANN), the linear regression between trends and elevation found in the western side is associated with a wetting signal at high elevations, coherently with what is found in the TP and the GAR. No significant vertical stratification has been assessed on the eastern side of the ANN. In contrast, in the southern Andes (ANS), the distinctive knee-shaped profile is evident during summer but discernible even in the winter season. Comparing the elevational stratification of annual total precipitation trends to CRU and GPCC data (see the SI), the distributions exhibit a remarkable similarity to ERA5. They show the two branches of the distribution corresponding to the western and eastern sides of the Cordillera, even though this agreement vanishes in the binned profiles. Even though ERA5 may be considered as the most accurate precipitation dataset in the region (10°S - 30°S, Birkel et al. 2022), there is no specific literature on EDPC in South America to compare our results with.

For comprehensiveness, the entire analysis in each mountain area has been conducted also considering the relative trends of precipitation indices, by weighing temporal changes with their climatological values. The results obtained from this analysis align with those derived from the absolute trends, with some exceptions. The elevational distributions of index relative trends appear in many cases more compact, as the spatial variability of the indices climatological values is not factored into the trend analysis (e.g. R10mm for the RO - Figure S8a in the SI). In a few cases, this leads to significant elevational gradient values and slightly different binned profiles (e.g. R20mm for the GAR - Figure S8b in the SI). Table S1 in the SI summarises the results obtained evaluating the elevational gradients of precipitation indices, computed following the first approach (see Sect. 2).

Drawing overarching conclusions on the characteristics shared by the key mountain regions found with ERA5 reanalysis, the following considerations can be made:

1. The change of mean precipitation (Pm), heavy precipitation (R10mm), and the persistence of rainy conditions (CWD) show similar elevational profiles within each mountain region.
2. In the RO, in the GAR, and in the western side of the ANN, a simple linear regression can effectively describe EDPC, whereas the ANS and TP show a more complex elevational profile.
3. During the local summer season, the TP, GAR and the western side of the Andes, show a significant wetting signal (positive trend) at high elevations.

Understanding what drives the patterns of EDPC that we identified goes beyond the scope of this study, although some general features can be underlined. Precipitation rates may generally be expected to increase with elevation due to the dependence of condensation on the vertical uplift of air masses. Such orographic enhancement of precipitation can be attributed to thermodynamic and dynamic effects, which can exceed geographical variations in mountain precipitation due to a variety of synoptic atmospheric patterns. In a warming climate, this may explain the general tendency of a positive EDPC we found with this analysis.

The drivers behind the high-elevation wetting effect, which impact what has been found in all mountain chains except the RO, likely fall into the category of thermodynamic drivers. Primarily, the intensification of warming at higher elevations and its interconnected processes, such as the snow-ice albedo feedback, may contribute to the increase in local atmospheric water vapour, which in turn can lead to an enhancement of precipitation and

more pronounced precipitation extremes at higher elevations (Hu et al. 2021). Additionally, as noted by Guo et al. (2017), in the Tibetan Plateau, a reduction of near-surface wind speed has been highlighted to be more pronounced at high elevations. Changes in surface wind speed, the so-called "stilling" phenomenon, might impact local convection, potentially resulting in an increase in extreme precipitation at high elevations.

Concerning the results that has been found in the Rockies, it is plausible that dynamic drivers might supersede the thermodynamic ones, particularly given the complex topography of the area and the diversity of atmospheric patterns impacting the area. In fact, in this area precipitation is influenced by a wide range of circulation patterns, largely distinguished between the coastal and interior side of the mountain chain. Similarly to the Tibetan Plateau's drying impact resulting from modifications in the monsoon, further research should aim at examining the influence of large-scale changes (e.g., shifts in the jet stream and storm tracks) on the stratification found in the Rocky Mountains.

Our analysis of the elevational dependency of ERA5 precipitation and extreme precipitation change has revealed common patterns across global mountain areas that go beyond geographical variability. Such consistency in EDPC, something somehow unexpected for a complex variable as precipitation, will need to be confirmed thorough a further comprehensive comparative analysis with different observational datasets, and clearly prompts for interpretation with dedicated model studies.

Supplementary Information The online version contains supplementary material available at https://doi.org/10.1007/s00382-024-07328-6.

Author contributions All authors contributed to the study conception and design. The analysis of ERA5 data and the preparation of figures were carried out by OF. All authors participated in the interpretation and discussion of the results. OF and EA prepared the first draft of the manuscript and all authors contributed to further revised versions, read and approved the final manuscript.

Funding Open access funding provided by Università degli Studi di Torino within the CRUI-CARE Agreement. EA acknowledges funding from "Clim2FlEx - Mapping of climate to flood extremes" - PRIN Progetti di Rilevante Interesse Nazionale 2022 - COD. 2022AX3882 and "FuturClEsP - The future of climate extreme events and their impact in Piedmont" - CRT Foundation, II TORNATA 2022 - RIF. 2022.1724. EP acknowledges funding from the PRIN PNRR 2022 P202292C4C - Impact of LOCal conditions on the change of Italian microCLIMAtes (LocClima) - UE Funding - NextGenerationEU - mission 4, component 2, investment 1.1 - CUP: D53D23022780001

Code and data availability Available on request.

Declarations

Conflict of interest The authors have no relevant financial or non-financial interests to disclose.

Ethical approval Not applicable.

References

Archer DR, Fowler HJ (2004) Spatial and temporal variations in precipitation in the upper indus basin, global teleconnections and hydrological implications. Hydrol Earth Syst Sci 8(1):47–61. https://doi.org/10.5194/hess-8-47-2004

Beniston M (2003) Climatic change in mountain regions: A review of possible impacts. Climatic Change 59. https://doi.org/10.1023/A:1024458411589

Bibi S, Wang L, Li X, et al (2018) Climatic and associated cryospheric, biospheric, and hydrological changes on the tibetan plateau: a review. International Journal of Climatology 38(S1), https://doi.org/10.1002/joc.5411

Birkel SD, Mayewski PA, Perry LB, Seimon A, Andrade-Flores M (2022) Evaluation of reanalysis temperature and precipitation for the andean altiplano and adjacent cordilleras. Earth and Space Science 9(3):e2021EA001,934, https://doi.org/10.1029/2021EA001934

Caicedo P, Daniel J, Arias P et al (2020) Observed and projected hydroclimate changes in the andes. Frontiers in Earth Science 8. https://doi.org/10.3389/feart.2020.00061

Capecchi V, Pasi F, Gozzini B, Brandini C (2022) A convection-permitting and limited-area model hindcast driven by era5 data: precipitation performances in italy. Climate Dynamics 61. https://doi.org/10.1007/s00382-022-06633-2

Field C, Barros V, Stocker TF et al (2012) IPCC 2012: Managing the Risks of Extreme Events and Disasters to Advance Climate Change Adaptation. Cambridge University Press, Cambridge, United Kingdom and New York

Gimeno L, Dominguez F, Nieto R et al (2016) Major mechanisms of atmospheric moisture transport and their role in extreme precipitation events. Annu Rev Environ Resour 41:117–141. https://doi.org/10.1146/annurev-environ-110615-085558

Giorgi F, Torma C, EC, et al (2016) Enhanced summer convective rainfall at alpine high elevations in response to climate warming. Nature Geoscience 9. https://doi.org/10.1038/ngeo2761

Gobiet A, Kotlarski S, MB, et al (2014) 21st century climate change in the european alps-a review. Science of the Total Environment 493. https://doi.org/10.1016/j.scitotenv.2013.07.050

Goodison B, Louie P, Yang D (1998) Wmo solid precipitation measurement intercomparison. World Meteorological Organization-Publications-WMO TD 67

Guo X, Wang L, Tian L, Li X (2017) Elevation-dependent reductions in wind speed over and around the tibetan plateau. International Journal of Climatology 37. https://doi.org/10.1002/joc.4727

Hersbach H, Bell B, Berrisford P, et al (2023) Era5 hourly data on single levels from 1940 to present. Copernicus Climate Change

Service (C3S) Climate Data Store (CDS) https://doi.org/10.24381/cds.adbb2d47
Hu W, Yao J, He Q, Chen J (2021) Elevation-dependent trends in precipitation observed over and around the tibetan plateau from 1971 to 2017. Water (Switzerland) 13. https://doi.org/10.3390/w13202848
Immerzeel WW (2020) Importance and vulnerability of the world's water towers. Nature 577:364–369
Karl TR, Nicholls N, Ghazi A (1999) Clivar/gcos/wmo workshop on indices and indicators for climate extremes workshop summary. Clim Change 42(1):3–7. https://doi.org/10.1023/A:1005491526870
Kittel T, Thornton P, Royle J, Chase T (2002) Climates of the rocky mountains: Historical and future patterns. In: Fagerberg J, Mowery DC, Nelson RR (eds) Rocky Mountain Futures: An Ecological Perspective, Island Press, Covelo, CA., chap 4
Kochendorfer J, Rasmussen R, Mea W (2017) The quantification and correction of wind-induced precipitation measurement errors. Hydrol Earth Syst Sci 21:1973–1989. https://doi.org/10.5194/hess-21-1973-2017
Kotlarski S, Bosshard T, Lüthi D, Pall P, Schär C (2012) Elevation gradients of european climate change in the regional climate model cosmo-clm. Climatic Change 112. https://doi.org/10.1007/s10584-011-0195-5
Krishnamurti TN, Kishtawal CM (2000) A pronounced continental-scale diurnal mode of the asian summer monsoon. Mon Weather Rev 128(2):462–473. https://doi.org/10.1175/1520-0493(2000)128<0462:APCSDM>2.0.CO;2
Kuhn M, Olefs M (2020). Elevation-Dependent Climate Change in the European Alps. https://doi.org/10.1093/acrefore/9780190228620.013.762
Kumar PV, Naidu c, Prasanna K, (2020) Recent unprecedented weakening of indian summer monsoon in warming environment. Theoretical and Applied Climatology 140. https://doi.org/10.1007/s00704-019-03087-1
Kumar P, Patel A, Rai J et al (2024) Environmental challenges and concurrent trend of weather extremes over uttarakhand himalaya. Theor Appl Climatol 155:1217–1246. https://doi.org/10.1007/s00704-023-04690-z
Kumar P, Sharma K (2023) Snowfall shift and precipitation variability over sikkim himalaya attributed to elevation-dependent warming. Journal of Atmospheric Science Research 6(4):1–25, https://doi.org/10.30564/jasr.v6i4.5854
Lavers DA, Simmons A, Vamborg F, Rodwell MJ (2022) An evaluation of era5 precipitation for climate monitoring. Q J R Meteorol Soc 148(748):3152–3165. https://doi.org/10.1002/qj.4351
Li X, Wang L, Guo X, Chen D (2017) Does summer precipitation trend over and around the tibetan plateau depend on elevation? Int J Climatol 37(S1):1278–1284. https://doi.org/10.1002/joc.4978
Liu X, Cheng Z, Yan L, Yin ZY (2009) Elevation dependency of recent and future minimum surface air temperature trends in the tibetan plateau and its surroundings. Global Planet Change 68:164–174. https://doi.org/10.1016/j.gloplacha.2009.03.017
Li C, Yanai M (1996) The onset and interannual variability of the asian summer monsoon in relation to land-sea thermal contrast. Journal of Climate 9(2):358–375 https://doi.org/10.1175/1520-0442(1996)009<0358:TOAIVO>2.0.CO;2
Masson-Delmotte V, Zhai P, Pirani A, et al (2021) IPCC 2021: The Physical Science Basis. Contribution of Working Group I to the Sixth Assessment Report of the Intergovernmental Panel on Climate Change. Cambridge University Press, Cambridge, United Kingdom and New York, https://doi.org/10.1017/9781009157896
Midhuna T, Kumar P, Dimri A (2020) A new western disturbance index for the indian winter monsoon. J Earth Syst Sci 129(59), https://doi.org/10.1007/s12040-019-1324-1
Mukherjee S, Joshi R, Prasad R et al (2015) Summer monsoon rainfall trends in the indian himalayan region. Theor Appl Climatol 121:789–802. https://doi.org/10.1007/s00704-014-1273-1
Napoli A, Crespi A, Ragone F, Maugeri M, Pasquero C (2019) Variability of orographic enhancement of precipitation in the alpine region. Scientific Reports 9. https://doi.org/10.1038/s41598-019-49974-5
Napoli A, Pepin N, Palazzi E, Zardi D (2023) A workshop on advances in our understanding of elevation dependent climate change. vol 40, https://doi.org/10.1175/BAMS-D-23-0043.1
Palazzi E, Hardenberg J, Provenzale A (2013) Precipitation in the hindu-kush karakoram himalaya: Observations and future scenarios. J Geophys Res 118:85–100. https://doi.org/10.1029/2012JD018697
Palazzi E, Mortarini L, Terzago S, von Hardenberg J (2019) Elevation-dependent warming in global climate model simulations at high spatial resolution. Climate Dynamics 52. https://doi.org/10.1007/s00382-018-4287-z
Paul S, Ghosh S, Oglesby R et al (2016) Weakening of indian summer monsoon rainfall due to changes in land use land cover. Sci Rep 6. https://doi.org/10.1038/srep32177
Pepin NC, Arnone E, Gobiet A et al (2022) Climate changes and their elevational patterns in the mountains of the world. Reviews of Geophysics 60. https://doi.org/10.1029/2020RG000730
Pepin N, Bradley RS, Diaz HF et al (2015) Elevation-dependent warming in mountain regions of the world. Nature Climate Change 5. https://doi.org/10.1038/nclimate2563
Portner HO, Roberts D, Masson-Delmotte V et al (2019) IPCC 2019: Special Report on the Ocean and Cryosphere in a Changing Climate. Cambridge University Press, Cambridge, United Kingdom and New York
Potter E, Fyffe C, Aea Orr (2023) A future of extreme precipitation and droughts in the peruvian andes. Climate and Atmospheric Science 6. https://doi.org/10.1038/s41612-023-00409-z
Schär C, Davies TD, Frei C, Wanner H et al (1998) Current alpine climate. In: Cebon P, Dahinden U, Davies H, Imboden D, Jäger C (eds) Views from the Alps: regional perspectives on climate change. MIT Press, Boston, pp 21–72
Singh KSRP, Kumar N (1995) Topographic influence on precipitation distribution in different ranges of the western himalayas. Nord Hydrol 26:259–284. https://doi.org/10.2166/nh.1995.015
Storch Hv, Zwiers FW (1999) Statistical Analysis in Climate Research. Cambridge University Press
Sun H, Su F, Yao T, et al (2021) General overestimation of era5 precipitation in flow simulations for high mountain asia basins. Environmental Research Communications 3(12):121,003, https://doi.org/10.1088/2515-7620/ac40f0
Syed F, Giorgi F, Pal J et al (2006) Effect of remote forcings on the winter precipitation of central southwest asia part 1: observations. Theor Appl Climatol 86:147–160. https://doi.org/10.1007/s00704-005-0217-1
Toledo O, Palazzi E, Toro IMC, Mortarini L (2022) Comparison of elevation-dependent warming and its drivers in the tropical and subtropical andes. Climate Dynamics 58. https://doi.org/10.1007/s00382-021-06081-4
Treydte K, Schleser G, Helle G et al (2006) The twentieth century was the wettest period in northern pakistan over the past millennium. Nature 440:1179–82. https://doi.org/10.1038/nature04743
Valencia S, Marín DE, Gómez D et al (2023) Spatio-temporal assessment of gridded precipitation products across topographic and climatic gradients in colombia. Atmos Res 285(106):643. https://doi.org/10.1016/j.atmosres.2023.106643
Viviroli D, Archer DR, WB, et al (2011) Climate change and mountain water resources: Overview and recommendations for research, management and policy. Hydrology and Earth System Sciences 15. https://doi.org/10.5194/hess-15-471-2011

Yadav M, Dimri A, Mal S et al (2024) Elevation-dependent precipitation in the indian himalayan region. Theor Appl Climatol 155:815–828. https://doi.org/10.1007/s00704-023-04661-4

Yang K, Ye B, Dea Z (2011) Response of hydrological cycle to recent climate changes in the tibetan plateau. Clim Change 109:517–534. https://doi.org/10.1007/s10584-011-0099-4

Yao J, Yang Q, Mao W, Zhao Y, Xu X (2016) Precipitation trend-elevation relationship in arid regions of the china. Global and Planetary Change 143. https://doi.org/10.1016/j.gloplacha.2016.05.007